NANO LETTERS

2007
Vol. 7, No. 8
2234−2238

Dynamical Observation of Bamboo-like Carbon Nanotube Growth

Ming Lin,[†] Joyce Pei Ying Tan,[†] Chris Boothroyd,[†] Kian Ping Loh,[‡] Eng Soon Tok,[§] and Yong-Lim Foo*,[†]

Institute of Materials Research and Engineering, 3 Research Link, S11760, Singapore, Department of Chemistry, National University of Singapore, 3 Science Drive 3, S117543, Singapore, and Department of Physics, National University of Singapore, 2 Science Drive 3, S117542, Singapore

Received March 23, 2007; Revised Manuscript Received May 28, 2007

ABSTRACT

The growth dynamics of bamboo-like multiwalled carbon nanotubes (BCNTs) via catalytic decomposition of C_2H_2 on Ni catalyst at 650 °C was observed in real time using an in situ ultrahigh vacuum transmission electron microscope. During BCNT growth, the shape of the catalyst particle changes constantly but remains metallic and crystalline. Graphene sheets (bamboo knots) within the nanotube preferentially nucleate on the multistep Ni–graphite edges at the point where the graphene joins the catalyst particle, where it is stabilized by *both* the graphene walls *and* the Ni catalyst surface. The growth of a complete inner graphene layer growth prior to contraction of the Ni catalyst particle due to restoring cohesive forces will result in a complete BCNT knot whereas partial growth of the inner wall will lead to an incomplete BCNT knot.

The extraordinary thermal, electronic, magnetic, and mechanical properties of carbon nanotubes (CNTs) make them important materials for applications such as nanoelectronic devices, hydrogen storage devices, biological probes, atomic probes, optical switches, and fuel cells.[1−4] Depending on the arrangement of the graphene layers and the angle of the graphene layers to the tube axis, tubular carbon based nanostructures can be classified into four subgroups, namely, single-walled carbon nanotubes (SWNTs), multiwalled nanotubes (MWNTs), bamboo-like carbon nanotubes (BCNTs), and cup-stacked carbon nanofibers (CNFs).[5−9]

Despite substantial strides made in the development of new CNT based devices and prototypes for nanotechnological applications, a complete understanding of the growth mechanism of these C nanostructures is lacking as many of the proposed theories remain to be verified.[10−14] Among the common methods used for fabrication of CNTs, chemical vapor deposition (CVD) of CNTs is the process of choice for industrial adoption due to its scalability and low cost. In CVD growth, the C product formed is strongly dependent on the growth temperature, type of catalyst, size of the catalyst particles, and the gaseous precursors.[6−8] Often, CVD growth using the same experimental growth conditions yields different morphologies or types of tubes, making complete and detailed understanding of the reactions difficult. This is further exacerbated by the ambient pressure or low vacuum growth conditions that convolute data with contaminants, thus making the growth process more complex to comprehend. For C-based nanostructures, understanding growth pathways is therefore the basis for large-scale industrial production of high-quality CNTs with controlled helicity, length, and diameters for technological applications. We designed in situ experiments to replicate/mimic the real CVD environment, less the contamination effect by operating in a system with ultrahigh vacuum (UHV) base pressure. In situ UHV transmission electron microscopy (TEM) is an ideal tool for conducting growth experiments due to the possibility of real time observation at the nanometer scale.[15] It allows us to investigate the mechanisms and growth kinetics of CNT quantitatively. Helveg et al. is the first group to use in situ TEM to observe the growth of carbon nanotubes.[16] . Several in situ TEM studies of carbon nanostructures have been reported recently.[17−20] Using in situ UHV TEM, we recently provided direct dynamical evidence that SWNT formation is caused by the nucleation of a hemispherical cap, with an activation energy of E_a ∼2.7 eV, followed by a strain relaxation driven shape transition to a tubular growth mode.[21]

In this Letter, we present high-resolution imaging of typical BCNT structures which are produced in a conventional furnace, as well as the real-time observations of the BCNT growth process on a Ni−MgO catalyst by catalytic decomposition of C_2H_2 in an in situ UHV TEM. The CNT growth in UHV TEM was conducted at 650 °C, with C_2H_2 being leaked continuously into the microscope column to maintain a backfilled pressure of $\sim 8 \times 10^{-6}$ Torr. In order to minimize

* Corresponding author: yl-foo@imre.a-star.edu.sg.
† Institute of Materials Research and Engineering.
‡ Department of Chemistry, National University of Singapore.
§ Department of Physics, National University of Singapore.

10.1021/nl070681x CCC: $37.00
Published on Web 06/30/2007

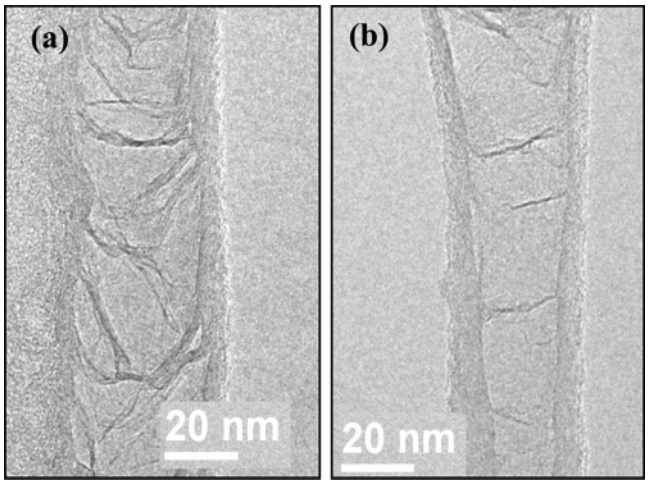

Figure 1. Postdeposition TEM images of typical BCNT with (a) complete and (b) incomplete kinks, which are grown using dc plasma enhanced small tube furnace (chemical vapor deposition). In this example, a 15 nm Ni film was first deposited on a SiO_2-coated Si(100) substrate. Prior to deposition, catalysts were treated in NH_3 flow for 5 min at 700 °C. And then the mixtures of 20 sccm C_2H_2 and 80 sccm NH_3 were introduced into the chamber, maintaining a pressure of 4 mbar. A −500 V bias was applied during reaction for the growth of straight BCNT.

the influence of electron beam on the growth process, the electron beam intensity was kept between 0.1 and 0.3 A/cm^2. Postdeposition inspection of C nanostructures showed no significant differences between irradiated and nonirradiated areas. The final carbon products formed in the TEM were strongly dependent upon the shape and size of the Ni catalyst supported on MgO. Among them, small Ni crystallites (<6 nm) catalyze the growth of the SWNTs through the base growth mode. Larger Ni particles, particularly with diameter ranging from 7 to 30 nm, tend to form mostly carbon nanocages and a few isolated MWNT/BCNT. Detailed information on the catalyst preparation and experimental procedures has been reported elsewhere.[21,22] On the basis of direct in situ experimental data, we elucidate the mechanism of both complete and incomplete knot formation in BCNT. The growth of a complete inner graphene layer prior to contraction of the Ni catalyst particle due to restoring cohesive forces will result in a complete BCNT knot whereas partial growth of the inner wall will lead to an incomplete BCNT knot. Our experiment and observation on heterogeneous gas−solid based reaction is different from those of solid−solid/liquid (carbon−metal) route for the formation of CNTs.[19,20] We believe the mechanism proposed here is representative of BCNT growth via CVD methods.

BCNTs are relatively straight-sided tubes divided into sections by "knots" made from single or multiple graphene sheets. From the morphological perspective, we can group the BCNT knots into two categories: (i) complete and (ii) incomplete knots. Figure 1a shows a typical BCNT grown by CVD ex situ in a furnace for high volume production. It has complete knots whereby the inner graphene compartment layers are fully formed, extended, and have bridged the inner diameter of the outer tube. Figure 1b shows, on the other hand, an incomplete bamboo knot structure. In order to

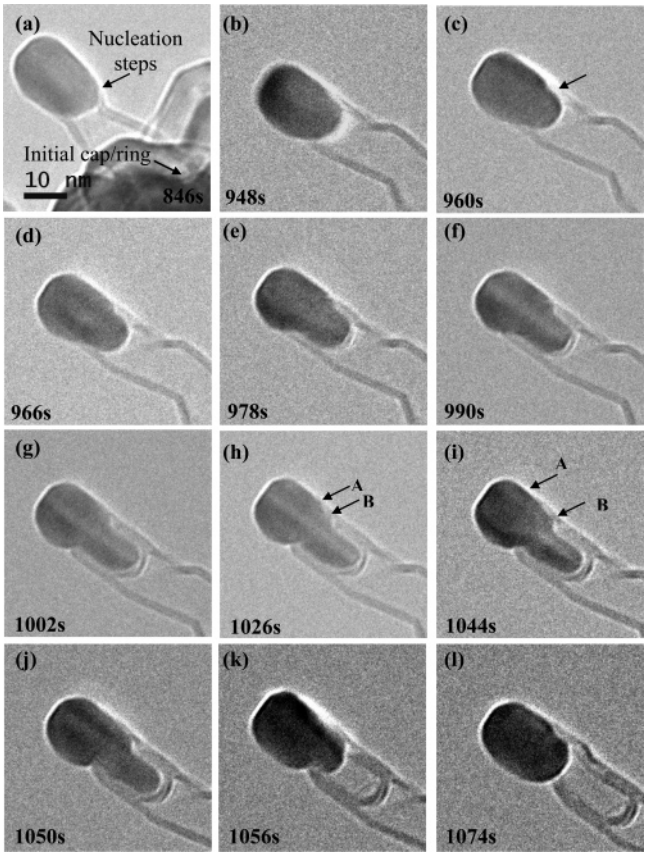

Figure 2. A sequence of in situ TEM images showing the growth of a bamboo-like carbon nanotube catalyzed by a Ni particle at 650 °C.

rationalize the difference in BCNT morphology and to control the types of BCNT structure formed during growth, i.e., complete or incomplete BCNT knots, we need to probe the BCNT growth mechanism.

The growth dynamics of BCNT were probed in situ using a sequence of bright-field images, taken at intervals of 6 s during exposure of the catalyst to C_2H_2 at an elevated temperature of 650 °C. Figure 2 shows a series of consecutive TEM images showing the formation of a knot in a BCNT catalyzed by a 12 nm Ni particle in real time (See Supporting Information, movie 1 (nl070681xsi20070528_071111.gif), which is grouped by a series of TEM images at 5 frames per second. One second in the video equals 30 s in the real experiment). Although the thermal vibration at 650 °C of the unsupported extended segment makes the images slightly unclear, we are still able to measure the length and thickness of the graphene wall and hence calculate both the number of graphene layers and the growth rate as function of time. The following important stages during growth were observed.

(i) The growth of *this* CNT does not start instantaneously upon opening the C_2H_2 leak valve. There is a time lag of 774 s before tube growth is observed.

(ii) The growth mode is tip-based. The catalyst particle remains as crystalline metallic Ni at 650 °C during the growth process (see Figure 1 in Supporting Information). Therefore, the mechanism of CNT growth is not through C precipitation from Ni_3C but rather through the diffusion of C adatoms

followed by nucleation and growth. There are two possible diffusion pathways, i.e., bulk diffusion and surface diffusion to the boundary of the Ni−graphene growth interface for growth of the outer graphene layer, with the latter dominating the reaction pathway due to a lower activation energy barrier and lower coordination number. For growth of inner graphene layers, we expect the interfacial diffusion of C adatom through the Ni−graphene edges/interface as the dominating route.

(iii) The front of the Ni particle has no graphene coating. Graphene layers parallel to the growth axis of the nanotube nucleate at the base of the symmetric Ni catalyst particle. The increase in the tube length thereafter is due to incorporation and attachment of C adatoms through surface diffusion at the *multistep* graphite−Ni edges. At this point the thickness of the carbon wall is ∼1.67 nm, corresponding to five graphene layers. The instantaneous growth rate measured is ∼0.34 nm s^{-1} (incorporation of ∼2500 C atoms per second).

(iv) As more C is added to the end of the graphene layers the Ni catalyst particle becomes asymmetric and the nucleation steps expand to become broader at the upper edge (indicated by the arrow in Figure 2c), as shown in parts b and c of Figure 2. This indicates the onset of the formation of the BCNT knot. Another five new graphene layers parallel to the as grown C walls are nucleated, resulting in a thicker wall as shown in Figure 2d. The newly formed layers are not observed on both sides of the Ni particle, indicating that the new graphite layers are asymmetric and do not encircle the whole Ni particle.

(v) As growth continues, the five newly nucleated graphene layers grow and extend around the bottom of the catalyst particle, thus forming a hemispherical cap within the nanotube and sealing the existing tube internally. This results in the formation of the knot in the BCNT, which fully encapsulates the lower part of the catalyst particle (panels e−g of Figure 2).

(vi) During BCNT formation, the effective diameter of the base of the catalyst shrinks, resulting in elongation of the Ni catalyst particle. This increases the effective surface and interface area of Ni catalyst particle. The elastic elongation also increases the strain energy of the catalyst.

(vii) The Ni particle contracts and is ejected from the newly formed bamboo knot. The complete growth process, i.e., (ii−vii) repeats yielding a complete BCNT with multiple knots along its length.

Nanotubes grown by CVD growth can be categorized into tip- and base-growth modes. This classification is based on the initial catalyst particle position prior to growth. For tip growth, the catalyst particle and the growth front move with respect to the initial catalyst position, whereas in the base-growth mode, C incorporation into graphene results in the walls being pushed away from the stationary catalyst to form the tubular structure. The growth front, in both cases, is at the catalyst−tube interface as shown in parts a and b of Figure 3. The nucleation and growth of CNT follow the adsorption−decomposition−surface diffusion−nucleation process. Nucleation and incorporation of C atoms into the growing graphite walls are driven by energetic considerations.[12,23,24] Hemispherical caps are found in the initial growth and nucleation of single-walled carbon nanotubes; similarly for the tip growth of MWNTs, closed caps have also been observed at some of the roots nanotubes (Supporting Information, Figure 2). It is interesting to note that when the leak valve is opened, we do not observe the immediate growth of CNTs. Instead, there is a period of ∼774 s where there is no discernible elongation of CNTs. Drawing on an analogy to the incubation period for critical nuclei in crystal growth, the initial formation of the hemispherical cap (precursor to the formation of the CNT outer wall) on the Ni catalyst is thus the slow step in the growth of the nanotube. Assuming an attempt frequency of 10^{13} s^{-1}, the estimated nucleation barrier for C adatoms to form the circular cap at 650 °C is 2.91 eV.

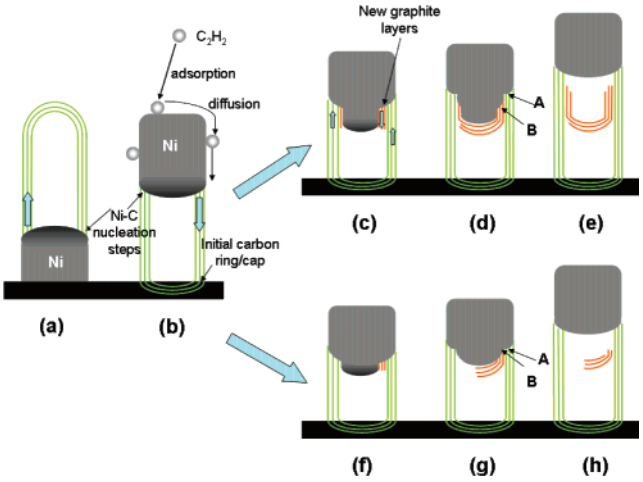

Figure 3. Schematic diagram showing (a) the growth of a CNT via the base-growth mode; (b) the growth of a CNT via the tip-growth mode; (c) the nucleation of a partial bamboo-knot graphite sheet at the graphene wall-catalyst junction; (d) the growth of the inner wall around the bottom of the Ni catalyst particle as adatoms are added to the inner wall edges through diffusion along the graphene−Ni interface; (e) subsequent formation of a hemispherical cap around the bottom of the catalyst particle. (Arrows indicate the direction of movement of the graphite relative to the Ni−graphite step edges; (e), (f), and (g) show formation of an incomplete knot.

Once an initial graphene layer forms on the Ni particle, the C adatoms on the Ni surface can further lower the system energy through incorporation into graphene layers.[24] The elongation thereafter is due to the incorporation and attachment of C adatoms to the interface between the initial graphene layer and the catalyst particle by surface diffusion of C adatoms on the metallic Ni catalyst. From our observations, the growth of graphene layers occurs preferentially at the Ni surface *multistep edges*, where the graphene layers at the end of the nanotube are in contact with the Ni particle, as shown in Figure. 2. The fact that we do not observe the nucleation of graphene fragments on other exposed Ni surfaces during the whole growth process further suggests that the *multistep edge* site is the preferred growth front. It has been noted that the diffusion through the graphene layers is energetically unfavorable with energy >10 eV.[20] Therefore, the most probable C source for growth of

inner graphene layers is through interfacial diffusion, where carbon atoms diffuse through the Ni−graphene interface at the multistep edge. Analogous to the phase boundary between two material systems, the interface provides a low-energy diffusion pathway for surface C adatoms to diffuse through and be incorporated into the growing inner graphene layers at the multistep edge. The growth is also complemented by direct bulk diffusion through Ni catalyst. However, we believe the latter is the minor diffusion pathway as the barrier is higher. During growth, the Ni *multistep edges* recede while the graphene sheet advances and the shape of the catalyst is *always* changing. This results in continuous elongation of the catalyst particle along the direction of growth. The elastic elongation of the catalyst caused by reduced internal radius of the tube increases its strain energy. Therefore, this suggests that the increase in graphene−Ni interfacial energy and strain energy during graphene layer formation is offset by the reduction in energy needed in forming graphene layers from an aggregate of isolated C adatoms on the Ni surface, when the tube is constrained to grow.

At the onset of formation of the bamboo-like structure, the growth front at the Ni−graphite steps abruptly changes into a two-step growth process (Figure 3). Step A yields the outer graphene wall, while step B forms the inner hemispherical cap round the base of the Ni particle. In both cases, the growth front still remains at *the multistep edge*. At the step A edge, the outer graphene layers continue to grow through the receding Ni step edges elongating the tube. Whereas at the step B edge, an extra graphene layer nucleates at the inner edge of the external tube wall next to the catalyst particle (indicated by arrow B in Figure 3c). This site is preferred because it is stabilized by interaction with *both* the external graphene wall *and* the Ni catalyst particle surface.[25] The graphene−graphene interplaner cohesive energy is ∼0.042 eV/atom[23] and the graphene−Ni binding energy ∼0.05 eV/atom.[26] Once the inner graphene sheet nucleates at the step B edge, C adatoms are continuously added to the inner wall edges through interfacial diffusion along the graphene−Ni interface.[15] The inner wall quickly grows around the bottom of the Ni catalyst particle, resulting in the formation of a hemispherical cap around the bottom of the catalyst particle. There are two possible pathways by which the inner wall can grow: (i) the C atoms continuously attach to the inner graphene layer at the multistep edge, resulting in the inner graphene layer being pushed away from the multistep edge and sliding round to encircle the bottom of the catalyst and (ii) C atoms diffuse along the Ni−graphene interface and add to the end of the inner graphene layer that is furthest away from the Ni multistep edge, requiring no sliding but a longer diffusion path. For both mechanisms the inner wall quickly grows around the bottom of the Ni catalyst particle, resulting in the formation of a hemispherical cap. Unfortunately in our experiments, we are not able to discern between these two mechanisms as this would require a tracer on the inner graphene layer.

From the growth perspective, considering the growth of the outer carbon walls, the growth front moves upward with reference to the static outer wall, like for the conventional tip-growth process where the catalyst particle moves with respect to the growth front. Growth of the BCNT knot, using the growth front at step B as a reference, therefore appears to follow the convention of base growth where the apparent inner tube growth direction is opposite of the other tube, as indicated in parts c and d of Figure 3. The completion of step B growth before the contraction of the Ni catalyst particle due to the restoring cohesive forces will result in a complete BCNT knot as illustrated in Figure 1a, whereas partial growth of the inner wall will lead to incomplete BCNT knots. Figure 4 shows a sequence of bright-field TEM images of an incomplete BCNT knots growth process. The rapid contraction of the Ni catalyst before the completion of growth of inner layers, results in leaving a partial knot behind. (Video 2 (nl070681xsi20070528_071211.gif) in Supporting information gives another example of incomplete knot formation.) This process is illustrated schematically in parts f−h in Figure 3. In order to form BCNT structures with complete knots in a controlled manner, the relative growth rate of the outer graphene layer and the inner BCNT layers is therefore of importance for kinetic considerations. We would expect complete BCNT knots to form if the contraction of the Ni catalyst particle occurs after the growth of the inner hemispherical cap is completed.

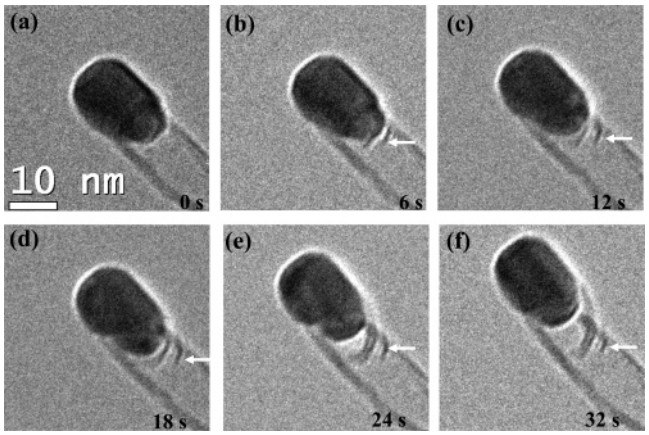

Figure 4. A sequence of TEM images showing the formation of an incomplete knot in less than 6 s. The fast restoring action of Ni catalyst leaves an incomplete knot behind. White arrows indicate where knot is formed. The time on (c)−(f) is referenced to frame (a), which is set to 0 s.

In summary, we have used in situ TEM to probe the growth mechanism of the BCNT structure, in particular the knot formation process. The catalyst particle remains metallic and crystalline during exposure to C_2H_2. Therefore, BCNT growth follows the adsorption−decomposition−surface diffusion−step nucleation process instead of a precipitation reaction. During BCNT growth, the shape of the catalyst particle changes constantly. The BCNT knot preferentially nucleates on the multistep Ni−graphite edges, at the graphene wall−catalyst junction, as it is stabilized by *both* the graphene walls *and* the Ni catalyst surface. A complete inner graphene layer growth prior to contraction of the Ni catalyst particle due to restoring cohesive forces will result in a complete BCNT knot whereas partial growth of the inner wall will lead to an incomplete BCNT knot.

Supporting Information Available: Figures showing a selected area diffraction pattern of Ni-MgO catalyst during and after CNT growth and bright field TEM images of BCNTs and videos showing the formation of complete and incomplete BNCT knots. This material is available free of charge via the Internet at http://pubs.acs.org.

References

(1) Saito, R.; Dresselhaus, M. S.; Dresselhaus, G. *Physical Properties of Carbon Nanotubes*; World Scientific Publishing: Singapore, 1998.
(2) Dresselhaus, M. S.; Dresselhaus, G.; Avouris, Ph. *Carbon Nanotubes*: *Synthesis, Structure, Properties, and Applications*; Springer: Berlin, 2001.
(3) Krishnan, R.; Nguyen, H. Q.; Thompson, C. V.; Choi, W. K.; Foo, Y. L. *Nanotechnology* **2005**, *16*, 841.
(4) Zhu, Y. W.; Elim, H. I.; Foo, Y. L.; Yu, T.; Liu, Y. J.; Ji, W.; Lee, J. Y.; Shen, Z. X.; Wee, A. T. S.; Thong, J. T. L.; Sow, C. H. *Adv. Mater.* **2006**, *18*, 587.
(5) Iijima, S. *Nature* **1991**, *354*, 56.
(6) Zhang, G.; Mann, D.; Zhang, L.; Javey, A.; Li, Y.; Yenilmez, E.; Wang, Q.; Mcvittie, J. P.; Nishi, Y.; Gibbons, J.; Dai, H. *Proc. Natl. Acad. Sci. U.S.A.* **2005**, *102*, 16141.
(7) Kong, J.; Soh, H.; Cassell, A. M.; Quate, C. F.; Dai, H. *Nature* **1998**, *395*, 878.
(8) Ren, Z. F.; Huang, Z. P.; Xu, J. W.; Wang, J. H.; Bush, P.; Siegal, M. P.; Provencio, P. N. *Science* **1998**, *282*, 1105.
(9) Katayama, T.; Araki, H.; Yishino, K. *J. Appl. Phys.* **2002**, *91*, 6675.
(10) Little, R. B. *J. Cluster Sci.* **2003**, *14*, 135−185.
(11) Baker, R. T. K. *Carbon* **1989**, *27*, 315.
(12) Hofmann, S.; Csanyi, G.; Ferrari, A. C.; Payne, M. C.; Robertson, J. *Phys. Rev. Lett.* **2005**, *95*, 036101.
(13) Ding, F.; Rosen, A.; Bolton, K. *J. Phys. Chem.* **2004**, *108*, 17369.
(14) Cui, H.; Yang, X.; Simpson, M. L.; Lowndes, D. H.; Varela, M. *Appl. Phys. Lett.* **2004**, *84*, 4077.
(15) Kodambaka, S.; Hannon, J. B.; Tromp, R. M.; Ross, F. M. *Nano Lett.* **2006**, *6*, 1292.
(16) Helveg, S.; Lopez-Cartes, C.; Schested, J.; Hansen, P. L.; Clausen, B. S.; Rostrup-Nielsen, J. R.; Abild-Pedersen, F.; Norskov, J. K. *Nature* **2004**, *427*, 426.
(17) Hofmann, S.; Sharma, R.; Ducati, C.; Du, G.; Mattevi, C.; Cepek, C.; Cantoro, M.; Pisana, S.; Parvez, A.; Cervantes-Sodi, F.; Ferrari, A. C.; Dunin-Borkowski, R.; Lizzit, S.; Petaccia, L.; Goldoni, A.; Robertson, J. *Nano Lett.* **2007**, *7*, 602.
(18) Yasuda, A.; Kawase, N.; Banhart, F.; Mizutani, W.; Shimizu, T.; Tokumoto, H. *J. Phys. Chem. B* **2002**, *106*, 1849.
(19) Ichihash, T.; Fujita, J.; Ishida, M.; Ochiai, Y. *Phys. Rev. Lett.* **2004**, *92*, 215702.
(20) Rodriguez-Manzo, J. A.; Terrones, M.; Terrones, H.; Kroto, H. A.; Sun, L.; Banhart, F. *Nat. Nanotechonol.* **2007**, *2*, 307.
(21) Lin, M.; Tan, J. P. Y.; Boothroyd, C.; Loh, K. P.; Tok, E. S.; Foo, Y. L. *Nano Lett.* **2006**, *6*, 449.
(22) Tan, C. K.; Loh, K. P.; Thong, J. T. L.; Soh, C. H.; Zhang, H. *Diamond Relat. Mater.* **2005**, *14*, 902.
(23) Lee, J. L.; Park, J. *Appl. Phys. Lett.* **2000**, *77*, 3397.
(24) Xu, J.; Saeys, M. *J .Catal*. **2006**, *242*, 217.
(25) Ding, F.; Bolton, K.; Rosen, A. *J. Electron. Mater*. **2006**, *35*, 207.
(26) Palser, A. H. *Phys. Chem. Chem. Phys.* **1999**, *1*, 4459.

NL070681X